

**A Study of Small Angle Radiative Bhabha Scattering and Measurement of the
Luminosity at SLD***

Sharon Leigh White

Stanford Linear Accelerator Center
Stanford University
Stanford, CA 94309

SLAC-Report-684
December 1995

Prepared for the Department of Energy
under contract number DE-AC03-76SF00515

Printed in the United States of America. Available from the National Technical Information Service, U.S. Department of Commerce, 5285 Port Royal Road, Springfield, VA 22161.

* Ph.D. thesis, University of Tennessee, Knoxville TN 37996

**A STUDY OF SMALL ANGLE RADIATIVE BHABHA
SCATTERING AND MEASUREMENT OF THE
LUMINOSITY AT SLD**

**A DISSERTATION
PRESENTED FOR THE
DOCTOR OF PHILOSOPHY
DEGREE
THE UNIVERSITY OF TENNESSEE, KNOXVILLE**

**BY
SHARON LEIGH WHITE
DECEMBER, 1995**

To the Graduate Council:

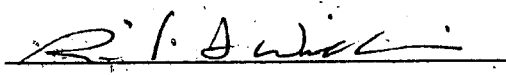
I am submitting herewith a dissertation written by Sharon Leigh White entitled "A Study of Small Angle Radiative Bhabha Scattering and Measurement of the Luminosity at SLD". I have examined the final copy of this dissertation for form and content and recommend that it be accepted in partial fulfillment of the requirements for the degree of Doctor of Philosophy with a major in Physics.



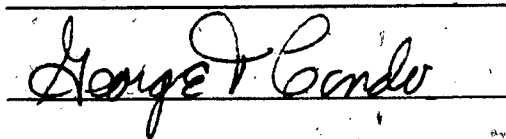
William M. Bugg, Major Professor

We have read this dissertation
and recommend its acceptance:










Accepted for the Council:



Associate Vice Chancellor
and Dean of The Graduate School

This dissertation is dedicated to my parents, Perry and Marguerite White.

Acknowledgements

As I reach the completion of my degree, there are many people I want to thank for their help along the way. First I would like to thank my advisor, Bill Bugg, who has taught me a great deal and has provided guidance throughout the process of completing my degree despite a very busy schedule as department head. I would also like to thank the other members of my committee, George Condo, Tom Handler, Bennie Ward, and Richard Williams for reading my dissertation and providing many useful comments and suggestions. In particular I'd like to thank Bennie Ward, co-author of the BHLUMI Monte Carlo program used throughout this dissertation, for many useful discussions about the use of BHLUMI. I would also like to thank Joe Hargis for the many hours he spent running BHLUMI events through the full shower simulation.

The luminosity monitor was the responsibility of the University of Oregon and the University of Tennessee, and I want to thank the members of these groups for the design, construction and operation of the SLD luminosity monitor - Steve Berridge, Bill Bugg, Rob Kroeger, and Achim Weidemann from Tennessee, and Jim Brau, Ray Frey, Koichiro Furuno, Jenny Huber, Hyun Hwang, Matt Langston, Hwanbae Park, Kevin Pitts, and Cary Zeitlin from Oregon. In particular I want to thank Kevin Pitts for many useful discussions about luminosity measurement and for providing me with luminosity monitor figures for this dissertation. I would also like to thank Hwanbae Park for helpful advice on SLD code. The SLD experiment could not operate without the extraordinary efforts of many people and I'd like to thank the entire SLD and SLC collaborations. This work was supported in part

by U.S. Department of Energy grant number DOE DE-FG05-91ER40627.

In the final stages of the preparation of this dissertation I received much helpful advice from three Tennessee students who preceded me in the completion of their degrees; Kathy Danyo Blackett, Gavin Blackett, and Murali Pisharody.

Finally, the support of family and friends helped to sustain me in my years of graduate study. I would especially like to thank my parents, Perry and Marguerite White, and my sister, Sarah White, for their continual support and encouragement. They always knew I could do it.

Abstract

Small angle Bhabha scattering ($e^+e^- \rightarrow e^+e^-$) is used to measure the luminosity for the 1993 run of the SLD experiment. SLD operates at the Stanford Linear Collider at Stanford Linear Accelerator Center where electrons and positrons are collided at center of mass energy on the Z^0 resonance. A silicon tungsten luminosity monitor is used to record the Bhabha events and a description of this device and its performance is presented. The luminosity is measured using two different methods to correct for small displacements in the luminosity monitor and the results are:

$$\mathcal{L} = 1726.5 \pm 5.1_{stat} \pm 3.9_{sys} \pm 4.6_{MC} \text{ nbarn}^{-1}$$

$$\mathcal{L} = 1718.5 \pm 5.0_{stat} \pm 2.2_{sys} \pm 5.5_{MC} \text{ nbarn}^{-1}$$

Measurement of the integrated luminosity is essential for the determination of the cross section for all final states in the experiment.

Radiative Bhabha events are studied using two types of radiative events; those with a photon visible in the luminosity monitor, and events with an undetected photon radiated down the beampipe, i.e. less than 28 mrad. The measured cross sections for these types of events in the acceptance region of the luminosity monitor are compared with Monte Carlo predictions from the BHLUMI 2.01 Monte Carlo. These cross sections are $\sigma_{sep\ photon} = 0.644 \pm 0.019_{stat} \pm 0.013_{sys} \pm 0.003_{lum} \text{ nbarn}$ for the events with an identifiable photon in the luminosity monitor, and $\sigma_{beampipe} = 7.45 \pm 0.22_{sys} \pm 0.07_{stat} \pm 0.03_{lum} \text{ nbarn}$ for events with a photon down the beampipe. Characteristics of the radiative events including photon energy distribution and acollinearity distributions are compared with the BHLUMI predictions.

Contents

1	Introduction	1
2	Theory	3
2.1	Introduction to the Standard Model	3
2.2	Theoretical Framework of the Standard Model	4
2.3	Fermions	6
2.4	Z^0 Production and Decay at e^+e^- Colliders	7
2.5	Introduction to Bhabha Scattering	8
2.6	Lowest Order Contributions to Bhabha Scattering	9
2.7	Radiative Corrections	11
3	SLC and SLD	14
3.1	Introduction	14
3.2	SLC	15
3.2.1	The Collider	15
3.2.2	Polarized Electron Source	16
3.3	SLD	17
3.3.1	Introduction	17
3.3.2	Polarimetry	19
3.3.3	Tracking	23
3.3.4	Particle Identification	27
3.3.5	Calorimetry	30

4	SLD Luminosity Monitor	35
4.1	Introduction	35
4.2	Operating Principles of Silicon Detectors	36
4.3	Luminosity Monitor Design	36
4.4	Luminosity Monitor Performance	44
4.4.1	Energy Resolution	44
4.4.2	Resolution in θ and ϕ	56
5	Luminosity Measurement	72
5.1	Introduction	72
5.2	Principles of Luminosity Measurement	73
5.3	Method	73
5.4	Event Selection	75
5.4.1	Trigger	75
5.4.2	Event Classification	77
5.5	Gross-Precise Method	83
5.6	Precise-Precise Method	86
5.7	Cross Section Determination	94
5.8	Systematic Errors	99
5.8.1	Systematic Errors in Gross-Precise Calculation	99
5.8.2	Systematic Errors Affecting the Precise-Precise Method	108
5.9	Results	110
6	Small Angle Radiative Bhabha Scattering	112
6.1	Introduction	112
6.2	Event Selection for Events with Visible Photons in the LMSAT	113
6.3	Monte Carlo Cross Section for Events with Visible Photons	116
6.4	Comparison of BHLUMI With Data for Separate Photon Events	120
6.4.1	Systematic Effects for Separate Photon Events	121
6.4.2	Results of Cross Section Measurement	122

6.4.3	Acollinearity	123
6.4.4	Photon Energy	126
6.5	Radiative Events with Highly Forward Photons	126
6.5.1	Event Selection	126
6.5.2	Monte Carlo Cross Section Determination	133
6.6	Comparison of BHLUMI with Data for Events with Photons In the Beampipe	135
6.6.1	Systematic Effects for the Beampipe Photon Events	135
6.6.2	Cross Section Measurement	137
6.6.3	Acollinearity	138
6.7	Conclusions	139
7	Conclusions	141
	Bibliography	143
	Vita	150

List of Tables

1	Properties of the materials making up the LMSAT/MASiC	40
2	Materials making up the LMSAT/MASiC	44
3	Number of PP and GP events and the weighting factor resulting from solving $(N_{PP} + wN_{GP})_{undisplaced} = (N_{PP} + wN_{GP})_{displaced}$ for w	86
4	Classification of events for full shower vs. vector cuts for a total sample of 4552 events.	97
5	Corrections to raw number of precise-precise events	110
6	Corrections to raw number of precise-precise + $\frac{1}{2}$ gross-precise events	111
7	Corrections to raw number of separate photon events	123
8	Corrections to raw number of beampipe photon events	137

19	Front face of LMSAT showing SLD tower numbering for rings in theta.	43
20	Energy distribution for South LMSAT, using all Bhabhas used for luminosity measurement. A Gaussian fit gives $\sigma/E=4.99\%$	46
21	Energy distribution for South LMSAT, using only precise-precise events, and excluding identified radiative events and events near the gap between LMSAT halves. A Gaussian fit gives $\sigma/E=4.85\%$	48
22	Energy vs. phi before correction for local hardening effect. The top figure is North, the bottom figure is South.	49
23	Energy vs. phi after correction for local hardening effect. The top figure is North, the bottom figure is South.	50
24	Energy distribution of all Bhabhas in South LMSAT after correction factors are applied. A Gaussian fit gives $\sigma/E=4.34\%$	51
25	Energy distribution of Bhabhas excluding events with one end in inner ring, events near the gap, and radiative events, after correction factors are applied. A Gaussian fit gives $\sigma/E=4.0\%$	52
26	Energy distribution of Monte Carlo Bhabhas using all events. A Gaussian fit gives $\sigma/E=3.98\%$	54
27	Energy distribution of Monte Carlo Bhabhas excluding events with one end in inner ring, radiative events, and events near the gap. A Gaussian fit gives $\sigma/E=3.67\%$	55
28	Theta distribution using energy weighted mean for Monte Carlo in top figure and data in bottom figure.	57
29	Top plot shows energy weighted mean theta vs. real theta from Monte Carlo, and bottom plot shows "snake" corrected theta vs. real theta from Monte Carlo.	58
30	Theta distribution after "snake" correction for Monte Carlo events.	59
31	Real theta - snake corrected theta, Monte Carlo events.	60
32	Real theta - snake corrected theta, vs. snake corrected theta.	62

List of Figures

1	Tree level Feynmann diagrams for e^+e^- collisions at the Z^0 resonance.	8
2	Born level contributions to Bhabha scattering.	10
3	Lowest order radiative corrections, where (a) shows real emission, and (b) shows virtual corrections.	12
4	A simplified schematic of the SLC.	15
5	Isometric drawing of SLD detector.	18
6	Quadrant of the SLD detector.	20
7	SLD Compton Polarimeter.	21
8	SLD Vertex Detector.	23
9	CDC cell structure. The circles represent sense wires, the diamonds are guard wires, and the crosses are field shaping wires.	25
10	CDC superlayers. A denotes axial layers, U and V denote stereo layers.	26
11	Schematic of barrel CRID components.	28
12	Barrel CRID drift box.	29
13	LAC Barrel EM and HAD modules.	31
14	Plate and tile detail of a LAC barrel HAD module.	32
15	WIC section detail.	34
16	Side view of luminosity monitor (LMSAT) and medium angle silicon calorimeter(MASiC) assembly.	38
17	Front face of one plane of the LMSAT.	39
18	A single silicon wafer from the LMSAT.	41

33	Real theta - corrected theta using second correction, vs. corrected theta.	63
34	Second order corrected theta vs. actual theta.	64
35	Top plot shows Monte Carlo theta distribution for theta corrected using second correction, bottom plot is the same distribution for data. 66	
36	Distributions of real theta minus corrected theta where the corrected theta is energy ² weighted mean (top left), snake correction (top right), and second order correction (bottom). All distributions are fit to a Gaussian distribution, and the standard deviations are $\sigma = 0.79, 0.55,$ and $0.35,$ respectively.	67
37	Snake corrected phi vs. real phi, Monte Carlo	68
38	Difference between actual phi and snake phi, vs. actual phi, Monte Carlo.	69
39	Phi distribution using snake correction in Monte Carlo in top plot and data in bottom plot.	70
40	Distribution of snake corrected phi minus actual phi, Monte Carlo. Top figure is for single width phi bins, rings 52-54, fit to a Gaussian distribution with $\sigma = 0.92^\circ$. Bottom figure is for double width phi bins, rings 55 and 56, fit to a Gaussian with $\sigma = 1.4^\circ$	71
41	Distribution of energy as seen by the trigger for full shower Monte Carlo events.	76
42	North vs. South cluster energies for a sample of the 1993 Bhabha events.	78
43	Energy vs. theta for North LMSAT in the top picture and for the South LMSAT in the bottom picture.	79
44	Energy vs. phi for North LMSAT in the top picture and for the South LMSAT in the bottom picture.	80

45	Fractional change in luminosity with y displacement in the top picture and fractional change in luminosity with z displacement in the bottom picture, using the gross-precise method.	85
46	Monte Carlo phi distribution with no displacement, and y displacements of 1 mm, 2 mm, and 5 mm.	88
47	Fit of D/A to d, the displacement in the x direction for Monte Carlo events.	90
48	Distribution of phi of maximum tower for all 1993 data events, South (top) and North(bottom).	91
49	Fit of the function F vs. the z displacement.	93
50	Distribution of total energy in North and South LMSATs for random background events.	101
51	Distribution of cluster energy in North and South LMSATs for random background events.	102
52	North cluster energy vs. South cluster energy for random background events.	104
53	Cluster energy vs. phi in North and South LMSATs for random background events.	105
54	Cluster energy vs. theta in North and South LMSATs for random background events.	106
55	Acollinearity distribution of full shower Monte Carlo events passing all criteria for having a separate photon except for the acollinearity cut.	117
56	Acollinearity distribution of all luminosity Bhabhas. The histogram in the top figure is Monte Carlo vector events; the points are data. Monte Carlo is normalized to the data, which has 128,264 events. In the bottom figure 2005 full shower Monte Carlo events are shown in the histogram, normalized to data.	124

57	Acollinearity distribution of separate photon events. The top figure shows vector Monte Carlo in the histogram compared to data. The bottom figure shows full shower Monte Carlo in the histogram compared to data. Monte Carlo is normalized to the 1045 data events.	125
58	Photon energy distribution for separate photon events. The top figure shows vector Monte Carlo in the histogram compared to the points showing the data. The bottom figure shows full shower Monte Carlo in the histogram compared to data. Monte Carlo is normalized to the 1045 data events.	127
59	Photon energy distribution for separate photon events. Vector Monte Carlo smeared by the energy resolution is shown in the histogram, the points are data. Monte Carlo is normalized to the 1045 data events.	128
60	Energy distributions for the main cluster energy for events with a visible photon. The top figures show data and the bottom figures show full shower Monte Carlo.	129
61	Acollinearity distribution for BHLUMI vector events which have a photon of at least 5 GeV down the beampipe.	130
62	Acollinearity distribution for BHLUMI vector events which pass cuts for being a precise-precise or gross-precise event except they need not pass the $\Delta\phi$ cut.	132
63	Acollinearity distribution for data (points) and vector BHLUMI events (histogram) with a photon down the beampipe.	138
64	Energy distributions using the main clusters for North and South LMSATs for events with a photon down the beampipe. The top figures are data, the bottom figures are full shower Monte Carlo.	140